Nanoscale

Accepted Manuscript

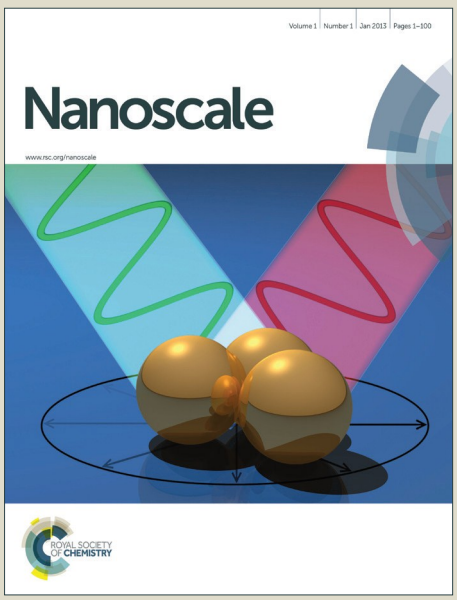

This is an *Accepted Manuscript*, which has been through the Royal Society of Chemistry peer review process and has been accepted for publication.

Accepted Manuscripts are published online shortly after acceptance, before technical editing, formatting and proof reading. Using this free service, authors can make their results available to the community, in citable form, before we publish the edited article. We will replace this *Accepted Manuscript* with the edited and formatted *Advance Article* as soon as it is available.

You can find more information about *Accepted Manuscripts* in the Information for Authors.

Please note that technical editing may introduce minor changes to the text and/or graphics, which may alter content. The journal's standard Terms & Conditions and the Ethical guidelines still apply. In no event shall the Royal Society of Chemistry be held responsible for any errors or omissions in this *Accepted Manuscript* or any consequences arising from the use of any information it contains.

ROYAL SOCIETY OF CHEMISTRY

www.rsc.org/nanoscale

Nanopatterned Polymer Brushes by Reactive Writing

Jonas F. Nawroth,[a] Claudia Neisser,[b] Artur Erbe,[b] Rainer Jordan[a]*

[a] Chair of Macromolecular Chemistry, School of Science, Technische Universität Dresden, Mommsenstr. 4, 01069 Dresden, Germany
[b] Institute of Ion Beam Physics and Materials Research, Helmholtz-Zentrum Dresden-Rossendorf, 01328 Dresden, Germany

author of correspondence: Rainer Jordan
E-mail: Rainer.Jordan@tu-dresden.de

ABSTRACT

Polymer brush patterns were prepared by a combination of electron beam induced damage in self-assembled monolayers (SAMs), creating a stable carbonaceous deposit, and consecutive self-initiated photografting and photopolymerization (SIPGP). This newly applied technique, reactive writing (RW), is investigated with *1H,1H,2H,2H*-perfluorooctyltriethoxysilane SAM (PF-SAM) on silicon oxide, which, when modified by RW, can be selectively functionalized by SIPGP. With the monomer *N,N*-dimethylaminoethyl methacrylate (DMAEMA) we demonstrate the straightforward formation of polymer brush gradients and single polymer lines of sub-100 nm lateral dimensions, with high contrast to the PF-SAM background. The lithography parameters acceleration voltage, irradiation dose, beam current and dwell time were systematically varied to identify optimal conditions for the maximum conversion of the SAM into carbonaceous deposit. The results of this approach were compared to patterns prepared by carbon templating (CT) under analogue conditions, revealing a dwell time dependency, which differs from earlier reports. This new technique expands the range of CT by giving the opportunity to not only vary the chemistry of the created polymer patterns with monomer choice but also vary the chemistry of the surrounding substrate.

Nanoscale Accepted Manuscript

INTRODUCTION

The modification of surfaces via polymer brushes is highly attractive to tailor the properties of interfaces. The fields of applications range from biotechnology to physics and material science.[1] While bringing preformed polymer chains in contact with a reactive surface (grafting-to) is a suitable approach,[2] the polymerization from the surface has some distinct advantages over grafting-to, such as higher grafting density and higher layers.[3]

For surface-initiated polymerizations (SIP) an initiator group has to be immobilized on the surface, which is routinely realized via self-assembled monolayers (SAM). The SAM either already bears the initiating functionality or is modified in a post self-assembly step.[4] In this manner, polymer brushes have been achieved by free[5] and controlled radical,[6] ring-opening metathesis,[7] living cationic[8] and living anionic polymerization.[9]

It is not only possible to create uniform coverage of SAMs, and therefore also polymer brushes, but there are various ways to pattern a surface in the micro- and nanometer range.[10-12] Patterning of polymer brushes allows exciting insights in numerous fields, e.g. in biology to study basic principles in cell surface interactions.[13]

Anyhow, one has to be aware that patterned polymer brushes, especially nanometer-sized features, do no necessarily behave like their homogenously grafted analog. Simulations by Patra and Linse[14] showed that brush heights universally scale with the size of the grafting area (footprint). Further, the outer parts of polymer brushes display different densities than the central part on top of the grafting area. To escape the osmotic pressure in the inner of the grafting area, brushes will extend over the latter. The amount of overlaying brushes depends on the ratio of the footprint (Δ) to the length of the polymer (N). With ratios $\Delta/N \geq 4$ the properties and lateral extension of the polymer brushes converge towards the values of homogenously grafted brushes. However, the central part of a nanopatterned brush shows similar properties to homogenously grafted brushes when a certain grafting density is reached.

Nanoscale Accepted Manuscript

These simulations were confirmed by Lee et al. [15] who investigated polymer features of 100-4000 nm size at different grafting densities and various polymerization times. It was found that the data from their AFM measurements fit the calculated scaling laws quite well.

Typically patterning processes such as microcontact printing (μCP),[16] nanoimprint lithography (NIL),[17] scanning probe lithography[18,19] photolithography or electron beam lithography (EBL)[20, 21] are applied. Except for μCP, these techniques rely on the application of resists or a combination of resists, which often makes the patterning a multi-step process of local modification and development steps.

As opposed to this, Schmelmer et al.[4] have shown that the formation of initiator patterns of nanometer size can be realized resist-free. 4'-nitro-1,1'-biphenyl-4-thiol (NBT) monolayers were directly irradiated by a focused electron beam, leading to crosslinking of the aromatic SAM and the chemical reduction of the terminal nitro group. The resulting areas of crosslinked 4'-amino-1,1'-biphenyl-4-thiol (cAMBT) were converted to 4'-azomethylmalonodinitrile-1,1'-biphenyl-4-thiol, which acted in a consecutive step as initiator for free radical polymerization (FRP). This process of electron beam chemical lithography (EBCL) not only leads to more stable monolayers, due to the cross-linking, but also to a high chemical contrast via the modified end group. Later, Steenackers et al.[22] showed that FRP from cAMBT can also proceed without further modification of the amino group, by using self-initiated photografting and photopolymerization (SIPGP). SIPGP is an initiator free polymerization that requires UV-irradiation, abstractable protons at the surface and was shown to be suitable for acrylic, methacrylic as well as styrenic monomers.[23,24] UV light excites the π electrons of the monomer to an exited singlet state that translates to a triplet state via inter system crossing. This triplet state is in an equilibrium with a biradical form of the monomer's double bond and the latter is capable of abstracting protons from the surface, generating a surface bound radical.[25] Earlier reports suggest that abstractable groups with

Nanoscale Accepted Manuscript

bond dissociation energies (BDEs) below 100 kcal/mol (418 kJ/mol)[26,27] to take part in this process.

SIPGP circumvents the lengthy introduction of suitable initiator functionalities and provides the ability to create a sharp chemical contrast for the formation of patterned brush surfaces if there is a sufficient difference for the BDEs.

Steenackers et al.[26] studied yet another approach of EBL to further investigate the potential of SIPGP. Electron beam induced carbon deposition (EBICD), usually an unwanted byproduct of every electron microscopic experiment, can also serve as initiating surface pattern. Residual hydrocarbons from the surface or the chamber vacuum are reduced on the surface under the irradiation of the beam. The carbonaceous deposit mainly consists of sp^2-carbon and roughly 10% sp^3-carbon species and forms on a variety of surfaces, such as Si, GaAs, nanocrystalline diamond or glass.[28] The C-H BDEs for sp^3-carbon of polycyclic sp^2-hydrocarbon precursors range from 80 to 301 kJ/mol,[29] so this method allows a direct patterning of surfaces and consecutive one-step SIPGP. With this method of carbon templating (CT) they were able to control the density of the EBICD by the applied electron dose. This was shown in experiments where dose gradients were written on surfaces. However, under the investigated conditions the deposit itself is usually roughly 1 nm in height; a detailed characterization by AFM is difficult, because of the low physical and topographical contrast of the EBICD to the surrounding surface. Nevertheless, conclusions about the quality of the EBICD can be drawn form the consecutive SIPGP. Because polymer brushes will stretch out with increasing grafting density, the quality of the underlying pattern will display as a height function of the polymer layer.[26] The measured height of the polymer brush pattern therefore can be controlled by the density of the deposit, if the SIPGP polymerization time (t_P) is kept constant.

To fine tune the chemical contrast on the surface even further one can also think about changing the chemistry of the non-irradiated area. A very common procedure is, as already

Nanoscale Accepted Manuscript

stated, to cover the surface with SAMs. However, there is a major drawback for SAM modification in the CT approach, the insufficient coverage. Usually, for oxide surfaces, prior to the self-assembly process, the surface is cleaned from residual organic impurities by either plasma or piranha treatment. This results in a clean, homogenous substrate and additionally in an increase of hydroxyl groups on the SiO_2 surface. A maximum amount of OH-groups eventually leads to the most densely packed silane SAM. Unfortunately, either of these treatments would also remove the EBICD. In contrast, a subsequent silanization would not cover the surface with maximum density because on the one hand the density of hydroxyl groups is lower and on the other hand the area around the initiator footprint is occupied by polymer brushes trying to wet the surface. Silanizing between EBCID and SIPGP could also be complicated, since common alkylsilanes used for hydrophobization, *e.g.* dichlorodimethylsilane, would also serve as initiator for SIPGP due to the low BDE, similar to the EBICD.

In contrast, SAMs from *1H,1H,2H,2H*-perfluorooctyltriethoxysilane (PF-SAM), display CF_2 or CF_3 groups at the interface and the high BDEs of F_3C-F and H_3C-F with 523 kJ/mol and 450 kJ/mol,[30] respectively, suggest that no surface bound radical will be formed under SIPGP conditions. Moreover, SAMs have been intensively investigated as EBL resists by Seshadri et al.[30] They irradiated an uniformly covered octadecylsilane (ODS) surface with a focused electron beam and did a variety of analytics. AFM measurements showed a height decrease in the irradiated areas that referred to a partial degradation rather than a complete ablation. The necessary electron dose for the maximum height decrease was found to be 0.5 mC/cm^2 after which the degradation leveled off and reached a plateau. Further, XPS and IR spectra revealed a decrease in carbon and hydrogen content in the irradiated ODS SAM, with an increasing amount of polar groups and cross-linking. The final residue was a stable carbonaceous film with a 30-40 % loss of carbon and hydrogen, in comparison to the non-irradiated ODS layer.

Nanoscale Accepted Manuscript

Our hypothesis is that the PF-SAM, which should be unreactive towards SIPGP conditions, due to its high BDEs, can be converted to carbonaceous deposit by electron beam induced damage. We describe here this technique as reactive writing (RW) and compare it to the CT approach.

RESULTS AND DISCUSSION

Scheme 1 shows the patterning process for the two applied methods of carbon templating (CT) and reactive writing (RW) of *1H,1H,2H,2H*-perfluorooctyl self-assembled monolayers (PF-SAM) on SiO_2 wafers. CT was performed as described in the literature.[18] Briefly, under electron beam irradiation carbon deposit is written directly onto the cleaned, unfunctionalized wafer surface. The substrate is immersed in bulk monomer and under UV irradiation DMAEMA is selectively polymerized in the patterned areas. In case of the RW, the oxide surface is activated by air plasma treatment, prior to PF-SAM formation. The homogenous PF-SAM is then degraded under electron beam irradiation, resulting also in carbonaceous residues. The consecutive SIPGP of DMAEMA again affects only the patterned areas. For a better comparison the identical layouts and conditions are investigated for both methods. The resulting polymer structures are analyzed by AFM under dry and ambient conditions in tapping mode.

Nanoscale Accepted Manuscript

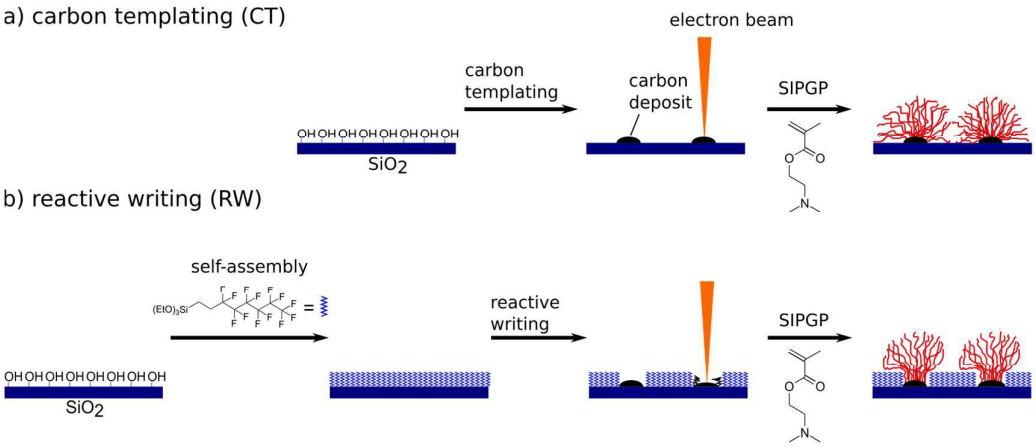

Scheme 1. Patterning process for a) carbon templating (CT) and b) reactive writing (RW).

To first test our assumption that the chosen PF-SAM is inaccessible towards surface grafting under SIPGP conditions, a model reaction is carried out. The setup is shown in Figure 1.

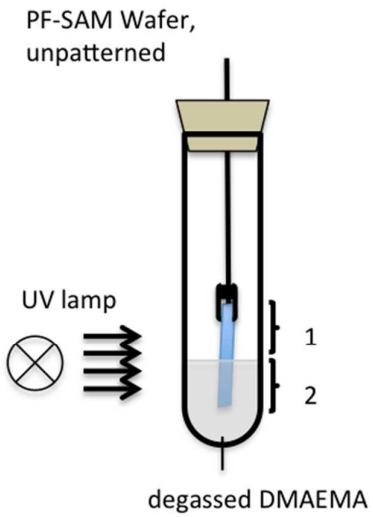

Figure 1. Experimental set-up of the control experiment to exclude SIPGP in non-patterned areas of the PF-SAM. A wafer piece covered with a homogeneous PF-SAM was partially immersed in bulk DMAEMA and irradiated by UV light.

The unpatterned, homogenously covered PF-SAM wafer is partially immersed in degased bulk monomer and irradiated by UV light for 2 h. After excessive cleaning of the substrate with ethanol and MilliQ water as well as extensive ultrasonication in both solvents, ellipsometry measurements did not show any increase in layer thickness, neither in comparison of the same area before and after irradiation, nor in comparison between the areas

Nanoscale Accepted Manuscript

1 and 2. To further quantify this result, XPS spectra of the areas 1 and 2 as well as a separate control sample were measured. The control sample was a 3-aminoproplysilane (APS) SAM on SiO_2, with SIPGP-grafted PDMAEMA brushes on the APS layer. The N1s signal at 402.6 eV that would arise from PDMAEMA was integrated for area 1, 2 and the control sample to 0.3 %, 0.7 % and 6.6 %, respectively. The rise of 0.4 % in the N1s signal from 1 to 2 could be assigned to either residual physisorbed DMAEMA or a measurement inaccuracy. However, the value is almost 10-fold smaller than the control and therefore we conclude that no polymerization takes place in non-irradiated areas of the PF-SAM.

Since the first assumption was validated, the second assumption that electron beam irradiation of PF-SAM results in carbonaceous deposit, was investigated. Therefore, rectangular (50x10 μm^2) electron dose gradients ranging from 0-100 mC/cm^2, 0-50 mC/cm^2 and 0-10 mC/cm^2 are created via RW, as well as CT to compare both techniques. Each gradient is the result of 100 stripes of 0.5x10 μm^2 size of linear increasing dose and each set of dose gradients is created at four different acceleration voltages of 2 kV, 5 kV, 10 kV and 20 kV. This results in a total of 12 gradients for RW and 12 for CT. It is noteworthy that these 12 gradients are on one single substrate, to minimize variations in reaction parameters.

However, the investigation of the structures after the writing process is challenging, due to low height differences and low physical contrast between irradiated and non-irradiated areas. Therefore we conclude the quality of the carbon deposit from the consecutive SIPGP. As known from literature, surface bound polymer brushes will stretch out as the grafting density increases. Polymer grafting density in SIPGP can be influenced by the irradiation time and thus, time of polymerization (t_P). Due to the free radical mechanism of SIPGP the polymer chain length is not significantly varied by t_P,[32] but the increasing brush grafting density leads to thicker polymer brush layers. Thus, if the polymerization parameters and dimensions of the pattern are otherwise unchanged, a higher polymer brush layer is the result of a higher

Nanoscale Accepted Manuscript

initiator/grafting point density on the surface. In our case the initiator functionality is simply an abstractable surface function in the carbon deposit.

Fig. 2 shows exemplary AFM height scans and the corresponding height profiles from the gradients written at 2 kV acceleration voltage for CT and RW, as well as a 3D representation of each 0-100 mC/cm^2 gradient. With 2 h the t_P was identical to the one in our first model reaction (Fig. 1). One can clearly see the amplification of the irradiated and the absence of polymer growth in the non-irradiated areas. The polymer brushes appear higher with increasing electron dose, suggesting a denser deposit beneath. A plateau in polymer brush height of about 200 nm is reached at around 50 mC/cm^2 for CT. These findings are in good agreement with previous studies and seem to be independent of monomer choice.[22] Furthermore, we see buckling at the edges of the polymer brush gradients, which is probably due to preferred interactions of the polymer brushes with each other, compared to the surrounding area and therefore differ from the region within the polymer brush pattern. In the case of the RW, the brush height seems to be less dependent of the applied dose. A plateau can be seen at 2 mC/cm^2, while doses above 10 mC/cm^2 seem to have a lowering effect. Additionally, we see unexpected high polymer brushes at the low energy dose end of each gradient for both methods that we cannot explain to date.

Nanoscale Accepted Manuscript

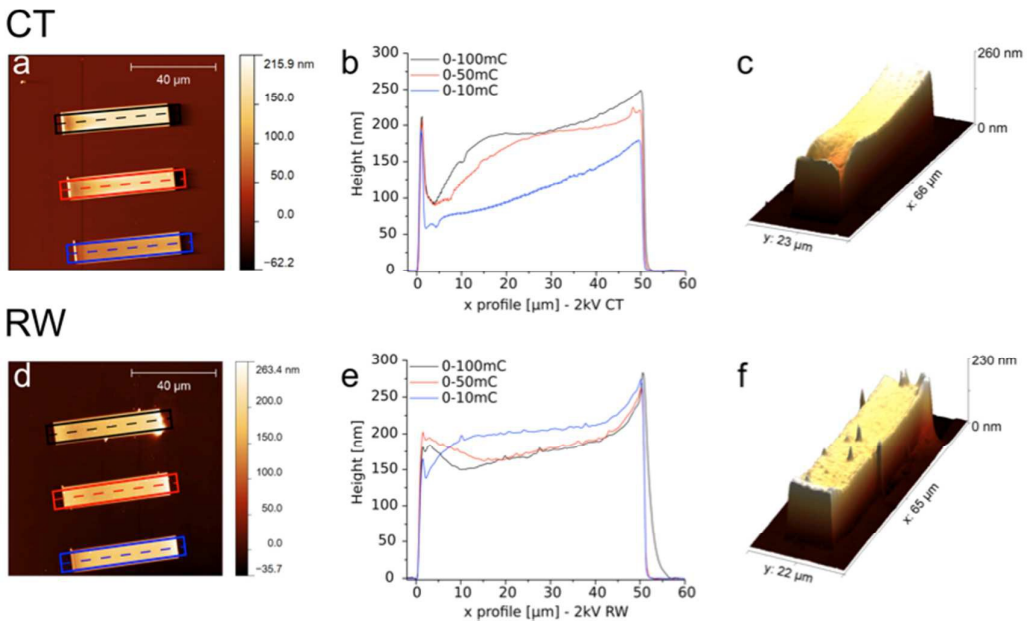

Fig. 2. 100 x 100 µm^2 AFM scans of polymer brush gradients created on 2 kV dose gradients (10 x 50 µm^2) by a) CT and d) RW. The corresponding height analysis along the indicated lines for b) CT and e) RW with 0-100 mC/cm^2 (black), 0-50 mC/cm^2 (red) and 0-10 mC/cm^2 (blue). c) and f) showing a 3D representation of the 0-100 mC/cm^2 gradient AFM scan for CT and RW, respectively.

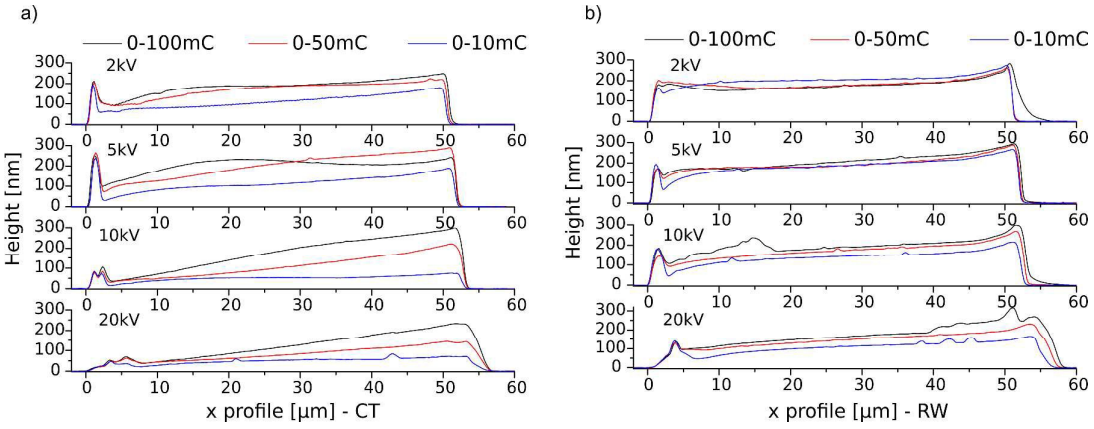

Fig. 3. AFM height profiles of the polymer brush gradient cross sections analogue to Fig. 2 as a function of the irradiation dose 0-100 (black), 0-50 (red) and 0-10 mC/cm^2 (blue) at different acceleration voltages (2, 5,10 and 20 kV) for a) CT and b) RW, t_P = 2 h.

In Figure 3 the height profiles of the polymer brush gradients are displayed in dependency of the acceleration voltage for both techniques. Under the very same polymerization conditions, features of equal dose but written with lower acceleration voltages result, after SIPGP, in higher polymer brush patterns. Therefore one can conclude a denser carbon deposit. This

Nanoscale Accepted Manuscript

trend is observed for either method and can be explained by a higher surface sensitivity with lower beam energies, due to a smaller penetration depth. The plateau region, where the brush height does not grow further with increasing dose, is not reached in all cases. For CT, as already shown in Fig. 2, this value is achieved at 50 mC/cm^2 at 2 kV, shifts to 80 mC/cm^2 for 5 kV and cannot be seen for higher voltages. There is, however, an unusual behavior at 5 kV, where the same dose in the 0-50 mC/cm^2 results in bigger polymer brush heights than for the 0-100 mC/cm^2. The origin of this is unclear. For RW the brush height seems to be less dependent on the applied electron dose. Again we can see that the plateau height shifts towards higher doses with increasing voltages, but the maximum height is reached in all four variations. The brush heights of around 200 nm in the plateau region are comparable in both methods showing similar behavior and good reproducibility of carbonaceous species.

As known from literature,[33] the energy needed to dissociate hydrocarbons is only a few eV, therefore all applied conditions from 2 kV to 20 kV are more than sufficient to create the contamination. In the case of CT, earlier experiments by Amman et al.[34] showed that the growth rate of the deposit from residual carbon precursors is mostly diffusion limited. Plotting the height over the dose then might not lead to the right conclusions. Looking into the writing parameters, the gradients do not only vary in acceleration voltage but also the beam current is changed, with larger currents for higher voltages (Tab. 1). If we now consider

$$D = \frac{I * t_{dwell}}{{d_{beam}}^2} \qquad (1)$$

with the area dose D, beam current I, dwell time t_{dwell} and beam diameter d_{beam}, it is obvious that for a diffusion based process the density of the carbon deposit is primarily dependent of the dwell time, if the minimal necessary dissociation energy of a few eV is applied (Fig. 3). As displayed in Table 1, to generate the same area dose at 2 kV and at 20 kV, the dwell time increases by more than a factor 4. Plotting the polymer brush height against the applied electron dose, as it has been done routinely, might not lead to the right conclusions for CT.

Nanoscale Accepted Manuscript

Tab. 1. Variation of the current and the resulting relative differences in dwell time for the four investigated acceleration voltages.

Acceleration Voltage	2 kV	5 kV	10 kV	20 kV
Current [pA]	28	44	73	120
Factor dwell time	4.24	2.72	1.63	1

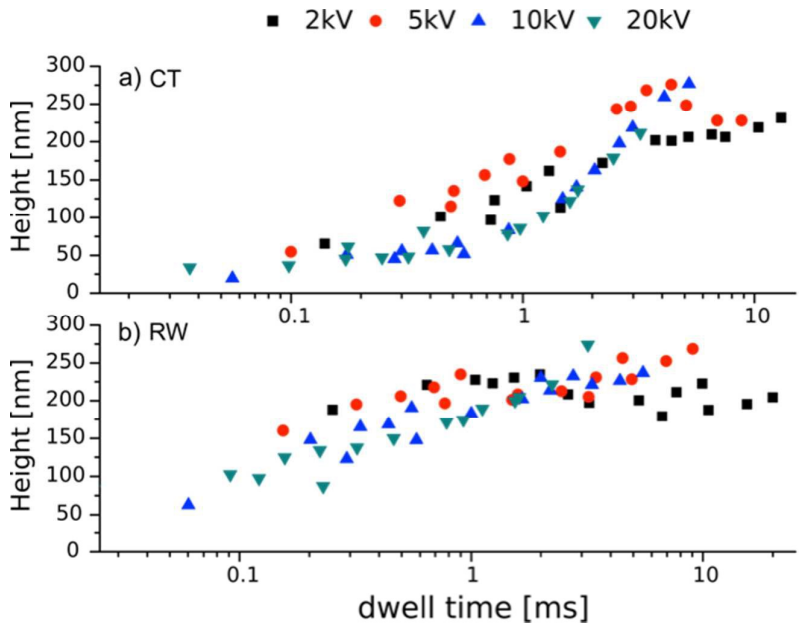

Fig. 4. Polymer brush heights in dependency of the dwell time and the different acceleration voltages, for the electron dose gradients created by a) CT and b) RW, $t_P = 2$ h.

Figure 4 shows the new correlation of polymer brush height with the dwell time and the assumption of a time dependency for CT is confirmed. RW seems to be less dependent on dwell time. The same dwell times for RW result in higher brushes and earlier plateaus compared to CT. This is most likely because of differences in precursor reservoir densities.

There are two different growth regimes for electron induced deposit. One is limited by the current density and independent of the precursor flux (electron limited regime – e.l.), the other is limited by the flux and independent of the current density (precursor limited regime – p.l.). It is known from literature that carbon precursors, as in our cases, fall into the p.l. regime.[35] However, we do not have a gas flux for our precursors but a steady reservoir throughout

Nanoscale Accepted Manuscript

irradiation. The only difference between RW and CT then is the precursor density. For RW a large amount of precursors (PF-SAM) covers the surface while for CT hydrocarbons are loosely spread over the surface. The incoming electron beam dissociates these and leads to a depletion of precursors in this area. The higher mobility and the bigger concentration gradient of precursor molecules lead to surface diffusion towards the beam.[35] Therefore we assume that although the CT curve appears sigmoidal and the RW curve looks asymptotic, the deposit growth mechanism is similar. The difference in dwell time dependency that can be observed in Fig. 4 is then a result of the shifted slope.

However, the trend within one method and varying acceleration voltages is less definite. The differences in polymer brush height are less consistent, but there is a slight increase with decreasing voltage. A possible explanation could be drawn form the interaction characteristic of electron beams with solid substrates.

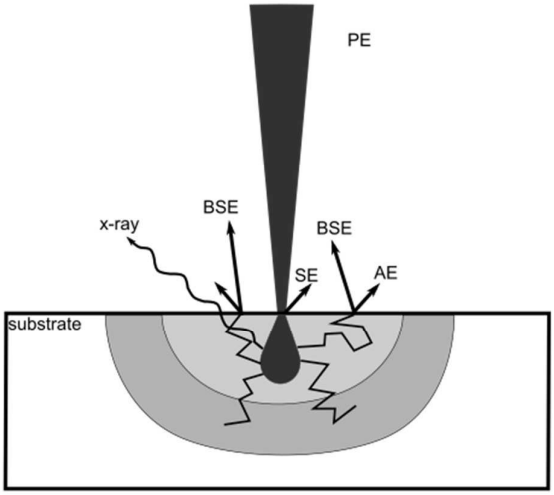

Fig. 5. Schematic of electron scattering upon substrate irradiation, with primary electrons (PE), backscattered electrons (BSE), secondary electrons (SE) and Auger electrons (AE). The different gray shades indicate electron density within the substrate in a qualitative manner. (Modified from L. Reimer, Scanning Electron Microscopy Springer-Verlag, Berlin, 1998)

Figure 5 shows a schematic of an electron beam scattering volume in an arbitrary substrate. The incoming primary beam does not exclusively realize the irradiation, but secondary

Nanoscale Accepted Manuscript

electrons (SE) from the substrate or back-scattered electrons (BSE) increase the illuminated area. The amount and energy of SE and BSE increases with acceleration voltage, which could be the reason for the decreased polymer brush heights at similar dwell times. However, 2 and 5 kV as well as 10 and 20 kV seem to be very similar to one another.

The amount of SE and BSE should not only be taken into consideration when it comes to the surface sensitivity of the primary beam, but as shown in Fig. 5, these electrons lead to wider structures in comparison to the areas which are covered by the primary beam. This results in parasitic carbon deposit growth or, for RW, degradation around the irradiation spot. Moreover, it is also well known that the amplification of surface patterns by polymer brushes leads to the widening of the resulting polymer feature.[7] The chain length of the tethered polymer brush limits the maximum widening of a surface structure. Therefore it can only be the initiator footprint size plus twice the brush length or less, depending on the chemical nature of the brush and the surface and the resulting wetting effects. The relative widening should be less pronounced the wider the footprint of the original pattern is compared to the polymer chain length. The dimensions of the investigated dose gradients are 50 x 10 μm^2, while the brush height in the plateau region indicated a length of roughly 200 nm. If the feature is written without parasitic irradiation, the width of the rectangles should not exceed 10.40 µm. Fig. 6 shows the width variation of the structure with the corresponding dwell time. The height profiles are measured along the y-axis, orthogonal to the profiles shown in Fig. 3. The data points are the result of five cross sections per acceleration voltage and dose gradient and are correlated to the corresponding dwell time in that part of the gradient.

Nanoscale Accepted Manuscript

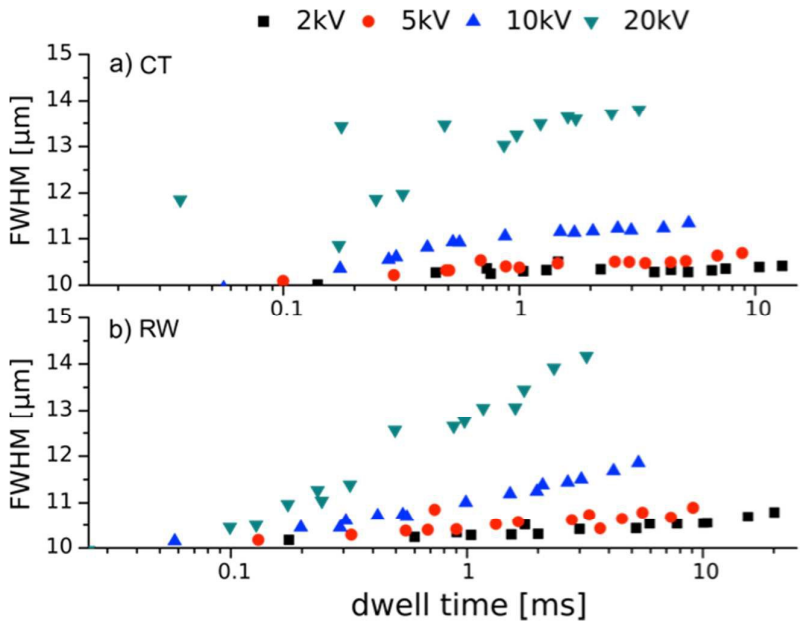

Fig. 6. Width of the 50 x 10 µm polymer brush gradients prepared from electron dose gradients as a function of the of the dwell time by a) CT and b) RW, $t_P = 2$ h.

Two trends can be observed for CT and RW. On the one hand the width of the polymer structure increases with increasing dwell time and on the other hand it also increases for higher acceleration voltages. This is the result of increasing penetration depth and therefore increasing SE and BSE yield. These lead to unwanted irradiation and widening of the intended structure,[35] which eventually also leads to polymerization in these areas.

The conclusion from these experiments is to use an electron beam of lower energy and to apply only small doses to the irradiated areas, which is controlled by the dwell time. This should result in narrow, yet dense carbon patterns for both methods.

To optimize the lateral resolution and minimize the lateral feature size of RW, a line array is written with 2 kV, 21 pA, 0.8 µs dwell time, 0.5 mC/cm^2 and 2 nm beam diameter. The same conditions are also applied for CT to compare both methods. AFM scans of these patterns are displayed in Fig. 7. DMAEMA was polymerized for 30 min to yield lower brush grafting densities and therefore smaller lateral dimension. Due to higher crowding of the brushes the height scales with larger footprints, as it was already shown by Lee et al.[7] and could also be observed in our experiments.

Nanoscale Accepted Manuscript

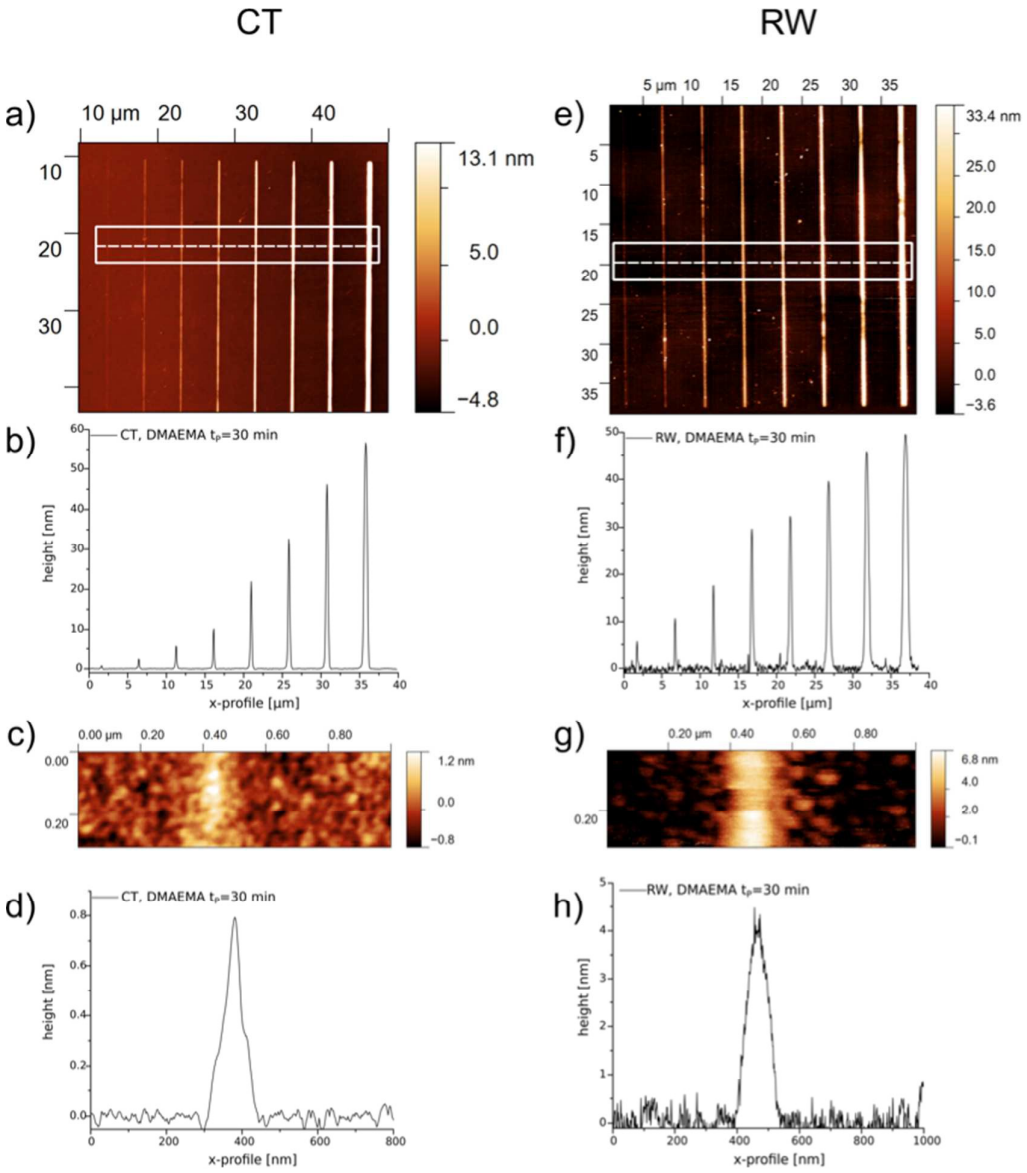

Fig. 7. AFM height scan of a line array created by CT a) and RW e) under optimized irradiation conditions (2 kV, 21 pA, 0.8 µs dwell time, 0.5 mC/cm^2, 2 nm beam diameter, t_P = 30 min). b) and f) The corresponding cross sections for the marked areas in the scans shown in a) and e). c) and g) Detailed scan of the narrowest line in a) and e). d) and h) The corresponding cross sections to the AFM scans c) and g), the profiles are the mean over the displayed scans.

Nanoscale Accepted Manuscript

Tab. 2. Height and full width at half maximum (FWHM) of the PDMAEMA brush line patterns displayed in Fig. 7. FWHM was determined by fitting the profiles with a Gaussian. The width of the footprint was not determined due to the low contrast of the carbon species to the background and therefore is replaced by the intended width. t_P = 30 min.
* Is the mean over 6 FWHM at 6 different positions along the line.

	CT		RW	
intended footprint [nm]	FWHM [nm]	Height [nm]	FWHM [nm]	Height [nm]
2	64*	0,7	98*	5
5	122	2	170	13
10	159	6	212	20
20	159	10	317	29
50	197	22	326	34
100	250	33	413	40
200	305	47	490	48
400	441	60	607	49

The height profiles determined from the AFM scans in Fig. 7 are fitted with a Gaussian curve to analyze the width of the single line features. The determined full width at half maximum (FWHM) are summarized in Tab. 2. Because of the issues of resolving the carbonaceous species prior to polymerization, the footprint of the structures is stated as the nominal width from the patterning software. However, it is possible for both methods to create polymer patterns with sub 100 nm dimensions. For the CT method, the minimal lateral dimension was determined to be 64 nm and therefore narrower as the feature at the same nominal footprint with RW. It is noteworthy that this could be realized at roughly a fifth of the brush height of RW, which directly translates into a lower grafting density for CT. From the values in Tab. 2 we can conclude that for low polymer brush heights CT and RW are comparable in their lateral dimension. At brush heights of about 30 nm, CT results in smaller widths than RW. This is probably due to the longer electron irradiation times needed to write larger features. The total amount of SE and BSE increases and the effect of carbon deposit conversion on a surface with higher precursor coverage would be more pronounced. It is noteworthy that polymer patterns with heights below 10 nm are of lower grafting density and thus most likely not in the brush, but in the mushroom regime.

Nanoscale Accepted Manuscript

A comparison of the lateral dimensions to earlier studies has to be seen critically, since in studies by Steenackers et al.[23] and Schmelmer et al.,[36] the investigated polymer brush was hydrophobic polystyrene in a glassy state while PDMAEMA as a hydrophilic polymer, swells under ambient conditions. This causes a better wetting of the surface by the polymer brush and results in broader patterns.

CONCLUSION

We report on a new technique, called reactive writing (RW), for the fabrication of nanopatterned polymer brushes on planar substrates. RW relies on the chemical degradation of alkyl silanes to carbonaceous species under electron beam irradiation and the amplification of these features by self-initiated photografting and photopolymerization (SIPGP). By choosing an appropriate self-assembled monolayer (SAM) that is inert towards radical abstraction during SIPGP, RW adds the possibility to change the substrates surface chemistry prior to the pattern formation and results in selective polymer brush growth. RW was investigated with respect to the applied acceleration voltage, electron doses as well as the dwell time and compared with the carbon templating (CT) method. Although it proved to be difficult to characterize the carbonaceous species for both methods because of the low chemical and physical contrast, the chemical reactivity of the carbonaceous layers in the consecutive SIPGP reaction allowed conclusions on the density of the formed deposits. The systematic variation of the writing parameters revealed new insights on the CT method, such as the strong dependency of the electron beam dwell time rather than to the pure electron dose, as stated in earlier reports. In contrast, RW is more tolerant towards the beam dwell time since the formation of the carbon deposit is not diffusion limited. The study further revealed that careful section of the writing parameters results in very dense carbonaceous species that are ideal two-dimensional templates to be amplified into nanopatterned polymer brush structures adding a third dimension by the brush layer thickness. Only with optimized

Nanoscale Accepted Manuscript

writing parameters, both RW and CT, give very similar nanopatterned polymer brushes at high grafting densities and with sub 100 nm resolution.

EXPERIMENTAL PART

Polished single-crystal silicon (100) wafers with 300 nm SiO_2 were purchased from MicroChemicals GmbH (Ulm, Germany). *N,N*-dimethylaminoethyl methacrylate (DMAEMA), *1H,1H,2H,2H*-perfluorooctyltriethoxysilane, toluene, ethylacetate (EtOAc) and ethanol (EtOH) were purchased from Sigma Aldrich (Steinheim, Germany) and used without further purification, unless otherwise stated. The stabilizing hydroquinone in DMAEMA was removed by aluminum oxide prior to use and remaining oxygen was removed by streaming inert gas through the bulk monomer for 30 min. Deionized water (Millipore, 18.2 MΩcm) water was used in all experiments.

Silicon substrates were cleaned prior to use by washing with toluene, EtOAc, EtOH, Millipore and then dried in a nitrogen stream. The dry substrates were treated with air plasma for 15 min and then rinsed with Millipore water and dried with a jet of dry nitrogen.

Following a procedure by Charlot et al.[37] the silanization was performed in the vapor phase. The wafer was placed in a glass chamber made from two petri dishes with four silane reservoirs (5 µL of the perfluorooctyltriethoxysilane) at the edges of the wafer. The chamber was closed and placed into a drying oven. The silanization was completed after 24 h at 80 °C, as determined by consecutive water contact angle measurements giving a static water contact angle of 109° which is consistent with the literature.[38]

Electron beam lithography (EBL) was done at a Raith 150^{TWO} with varying acceleration voltages, currents and doses. The gradients were the result of 100 0.5 x 10 μm^2 stripes with linearly increasing doses of 0-10, 0-50 and 0-100 mC/cm^2. The single lines were written at 2 kV acceleration voltage, 23 pA beam current, 0.8 µs dwell time and a nominal dose of 500

Nanoscale Accepted Manuscript

$\mu C/cm^2$. The designed writing sizes of the lines were 2, 5, 10, 20, 50, 100, 200 and 400 nm, respectively.

Self-initiated-surface grafting and surface polymerization (SIPGP) was performed in a Duran glass vial containing a degassed bulk monomer of DMAEMA in which the substrate was completely immerged and irradiated with an 8 W UV lamp (λ_{max} = 350 nm). The UV-irradiation time for gradients was 2 h, and for the single lines 30 min. After polymerization, the sample was intensively rinsed in EtOH and Millipore, followed by short ultrasonication in both solvents. Eventually, the samples were dried in nitrogen stream and stored under dry conditions.

Atomic force microscopy (AFM) was performed on a customized Ntegra Spectra RAMAN/AFM system from NT-MDT (Moscow, Russia) using standard tips for the gradients and ultrasharp DLC coated tips for the single lines. All measurements were done in tapping mode under dry, ambient conditions. The data were analyzed by the open source Gwyddion software package.

The presented data were obtained from arrays of nanopatterns prepared on two wafer pieces separately to ensure reproducibility and this for both, CT and RW, patterning methods. Each of the two wafers features arrays of three electron dose gradients ranging from 0-10, 0-50 and 0-100 mC/cm² for the four displayed acceleration voltages. Therefore each wafer pieces shows a total of twelve electron dose gradient arrays.

The height profiles (Fig. 2b, e and Fig. 3) were taken as an average of multiple lines over the course of the gradients structure, which was done with the help of the software Gwyddion. Therefore not a single pixel line but a line width corresponding to the width of the gradient was selected. For figures 4 and 6 the polymer brush gradients were measured orthogonal to the scanning direction represented in figure 2. Five cross section lines were equally distributed over the 3 dose gradients (0-10, 0-50 and 0-100 mC/cm²) and after converting the

Nanoscale Accepted Manuscript

position within the dose gradient in to the dwell time, 15 data points per acceleration voltage were achieved.

XPS analysis were performed using a ESCA5700 from Physical Electronics with a non-monochromatic Al Kα X-ray source (1486.6 eV). The X-ray source has a spot size of 200 µm and operates at a power of 250 W (13.0 kV and 19.2 mA). The spectra were taken by a hemi-spherical analyzer with pass energy of 93.90 eV and an energy step width of 0.125 eV. The base pressure was 8 x 10^{-10} mbar. Spectra were fitted by symmetric Voigt functions with a Shirley background correction.

Water contact angles were measured with the Drop Shape Analysis System DSA 10 from Krüss. An average of three different spots was taken for each sample. The measurements were performed at room temperature with bidestilled water and a drop size of 2 µL. The contact angles were obtained using the tangent method fitting.

Ellipsometry was performed with an SE800 ellipsometer from SENTECH

Instruments GmbH with a He–Ne laser (λ = 632.8 nm). The measurements were done at a fixed angle of incidence of 60° under ambient conditions. The spectra were modeled using the SpectraRay 3 software package. Each measurement is the average of three different spots per sample.

ACKNOWLEDGEMENT

We would like to thank R. Schubel for performing the XPS measurements.

The authors acknowledge the financial support by the Cluster of Excellence “Center for Advancing Electronics Dresden” (cfaed) and the Initiative and Networking Fund of the Helmholtz Association of German Research Centers through the International Helmholtz Research School for Nanoelectronic Networks, IHRS NANONET (VH-KO-606).

NOTES AND REFERENCES

Nanoscale Accepted Manuscript

1 Z. Nie and E. Kumacheva, *Nat. Mater.,* 2008, **7,** 277-290

2 K. Klaus, *Chem. Commun.,* 1996, 1025-1026

3 S. Edmondson, V.L. Osborne and W.T. Huck, *Chem. Soc. Rev.,* 2004, **33,** 14-22

4 U. Schmelmer, R. Jordan, W. Geyer, W. Eck, A. Gölzhäuser, M. Grunze and A. Ulman, *Angew. Chem. Int. Ed. Engl.,* 2003, **42,** 559-563

5 R. Laible and K. Hamann, *Adv. Colloid Interfac.,* 1980, **13,** 65-99

6 B. Zhao and W.J. Brittain, *J. Am. Chem. Soc.,* 1999, **121,** 3557-3558

7 W.K. Lee, K. C. Caster, J. Kim and S. Zauscher, *Small,* 2006, **2,** 848-853

8 R. Jordan and A. Ulman, *J. Am. Chem. Soc.,* 1998, **120,** 243-247

9 R. Jordan, A. Ulman, J.F. Kang, M.H. Rafailovich and J. Sokolov, *J. Am. Chem. Soc.,* 1999, **121,** 1016-1022

10 T. Chen, I. Amin and R. Jordan, *Chem. Soc. Rev.* 2012, **41**, 3280-3296

11 R. Ducker, A. Garcia, J. Zhang, T. Chen and S. Zauscher, *Soft Matter* 2008, **4**, 1774-1786

12 Q. Yu, L. K. Ista, R. Gu, S. Zauscher and G. P. López, *Nanoscale* 2015

13 X. Liu and S. Wang, *Chem. Soc. Rev.* 2014, **43**, 2385-2401

14 M. Patra and P. Linse, *Nano Lett.* 2006, **6**, 133-137

15 W.K. Lee, M. Patra, P. Linse and S. Zauscher, *Small,* 2007, **3,** 63-66

16 M. Husemann, D. Mecerreyes, C.J. Hawker, J.L. Hedrick, R. Shah and N.L. Abbott, *Angew. Chem. Int. Ed. Engl.,* 1999, **38,** 647-649

17 S.Y. Chou, P.R. Krauss and P.J. Renstrom, *J. Vac. Sci. Technol. B,* 1996, **14,** 4129-4133

18 M. Kaholek, W. K. Lee, B. LaMattina, K. C. Caster and S. Zauscher, *Nano Lett.,* 2004, **4,** 373-376

19 M. Kaholek, W. K. Lee, S. J. Ahn, H. Ma, K. C. Caster, B. LaMattina and S. Zauscher, *Chem. Mater.,* 2004, **16,** 3688-3696

20 A. Gölzhäuser, W. Eck, W. Geyer, V. Stadler, T. Weimann, P. Hinze and M. Grunze, *Adv. Mater.,* 2001, **13,** 806-809

Nanoscale Accepted Manuscript

21 S. J. Ahn, M. Kaholek, W. K. Lee, B. LaMattina, T. H. LaBean and S. Zauscher, *Adv. Mater.,* 2004, **16,** 2141-2145

22 M. Steenackers, A. Küller, S. Stoycheva, M. Grunze and R. Jordan, *Langmuir,* 2009, **25,** 2225-2231

23 M. Steenackers, A. Küller, N. Ballav, M. Zharnikov, M. Grunze and R. Jordan, *Small,* 2007, **3,** 1764-1773

24 N.A. Hutter, M. Steenackers, A. Reitinger, O.A. Williams, J.A. Garrido and R. Jordan, *Soft Matter,* 2011, **7,** 4861-4867

25 S. J. Li, C. G. Li, T. Li and J. J. Cheng, *Polymer Photochemistry Principles and Applications*, Fudan University Press, 1993

26 M. Steenackers, R. Jordan, A. Küller and M. Grunze, *Adv. Mater.,* 2009, **21,** 2921-2925

27 M.D. Allendorf, C.F. Melius, P. Ho and M.R. Zachariah, *J. Phys. Chem.,* 1995, **99,** 15285-15293

28 M. Steenackers, I.D. Sharp, K. Larsson, N.A. Hutter, M. Stutzmann and R. Jordan, *Chem. Mater.,* 2010, **22,** 272-278

29 K. May, S. Dapprich, F. Furche, B.V. Unterreiner and R. Ahlrichs, *Phys. Chem. Chem. Phys.,* 2000, **2,** 5084-5088

30 B.D. Darwent, *NSRDS-NBS NO. 31, U. S. DEPT. COMMERCE, WASHINGTON, D. C. JAN. 1970, 48 P,*

31 K. Seshadri, K. Froyd, A.N. Parikh, D.L. Allara, M.J. Lercel and H.G. Craighead, *J. Phys. Chem.,* 1996, **100,** 15900-15909

32 C. Barner-Kowollik, P. Vana, and T. P. Davis, 2002, The Kinetics of Free-Radical Polymerization, in Handbook of Radical Polymerization (eds K. Matyjaszewski and T. P. Davis), John Wiley & Sons, Inc., Hoboken, NJ, USA.

33 E.H. Hirsch, *Brit. J. Appl. Phys.,* 1960, **11,** 547-550

Nanoscale Accepted Manuscript

34 M. Amman, J.W. Sleight, D.R. Lombardi, R.E. Welser, M.R. Deshpande, M.A. Reed and L.J. Guido, *J. Vac. Sci. Technol. B,* 1996, **14,** 54-62

35 W. F. van Dorp and W. Hagen, *J. Appl. Phys.,* 2008, **104,** 081301

36 U. Schmelmer, A. Paul, A. Küller, M. Steenackers, A. Ulman, M. Grunze, A. Gölzhäuser and R. Jordan, *Small,* 2007, **3,** 459-465

37 A. Charlot, G. Souharce, J. Duchet-Rumeau and D. Portinha, *RSC Adv.,* 2013, **3**, 10497-10507

38 J. Genzer and K. Efimenko, *Science,* 2000, **290,** 2130-2133

TOC:

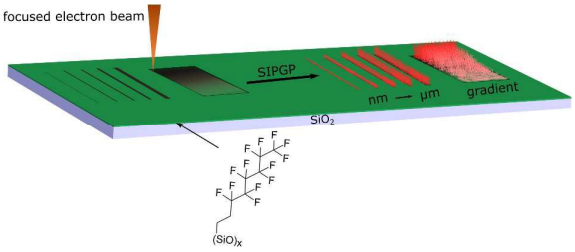

TOC entry:

A self-assembled monolayer of perflourinated silanes is used to prepare nanopatterned polymer brushes and brush gradients by focused electron beam reactive writing (RW) and surface-initiated photopolymerization of vinyl monomers.

Nanoscale Accepted Manuscript